Biosensors and Bioelectronics 146 (2019) 111753

Contents lists available at ScienceDirect

Biosensors and Bioelectronics

journal homepage: http://www.elsevier.com/locate/bios

Real-time monitoring of NADPH levels in living mammalian cells using fluorescence-enhancing protein bound to NADPHs

Amir Roshanzadeh [a], Hyuno Kang [b], Sung-Hwan You [a], Jaehong Park [a], Nguyen Dang Khoa [a], Dong-Hyun Lee [c], Geun-Joong Kim [c], Eung-Sam Kim [c,d,*]

[a] School of Biological Sciences and Biotechnology, Chonnam National University, Gwangju, 61186, Republic of Korea
[b] Korea Basic Science Institute Gwangju Center, Gwangju, 61186, Republic of Korea
[c] Department of Biological Sciences and Research Center of Ecomimetics, Chonnam National University, Gwangju, 61186, Republic of Korea
[d] Center for Next Generation Sensor Research and Development, Chonnam National University, Gwangju, 61186, Republic of Korea

ARTICLE INFO

Keywords:
Fluorescence enhancement
Metagenomic-blue fluorescent protein (mBFP)
NADPH-mBFP complex
Real-time imaging
Two-photon microscopy
Cell metabolism
Chemical inhibitors

ABSTRACT

Nicotinamide adenine nucleotide phosphate (NADPH) has been known to be involved in the multiple pathways of cell metabolism. However, conventional quantification assays for NADPH have required breaking down the cell membranes of around one million cells per assay, and monitoring NADPH flux in living cells has been limited by a few available tools. Here, we visualized NADPH levels in human cervical cancer cells HeLa using metagenome-derived blue fluorescent protein (mBFP), which specifically binds to NADPH and enhances the intrinsic fluorescence of NADPH up to 10-fold when imaged by two-photon microscopy to reduce photodamage. Adding an oxidizing agent such as diamide to HeLa cells that expressed mBFP led to an immediate decrease of intracellular NADPH depending on glucose availability in culture media. Furthermore, inhibiting glucose-6-phosphate dehydrogenase (G6PD) in the pentose phosphate pathway with dehydroandrosterone (DHEA) and knockdown of G6PD transcripts gradually decreased NADPH when diamide was added to living cells. These results demonstrate that introducing a bacterial mBFP gene into mammalian cells is a straightforward approach to monitoring intracellular NADPH flux in real time at the single-cell level. Moreover, this strategy can be expanded to tracking the spatio-temporal changes in NADPH even in single-cell organelles such as mitochondria and chloroplasts, which will allow us to more precisely assess the efficacy of biochemically or biophysically metabolic perturbations in animal and plant cells.

1. Introduction

Nicotinamide adenine dinucleotide phosphate is a ubiquitous coenzyme involved in numerous redox systems and living organisms (Dröge, 2002) existing in either reduced (NADPH) or oxidized ($NADP^+$) form. NADPH is widely used in cellular anabolism such as lipid, nucleotide, and macromolecular biosynthesis (Schulze and Harris, 2012; Smolke, 2009). Among several metabolic pathways in NADPH generation, pentose phosphate pathway (PPP) is a major source of NADPH in mammalian cells in which glucose-6-phosphate dehydrogenase (G6PD) converts $NADP^+$ to NADPH (Patra and Hay, 2014). Cells from normal tissues mainly generate their energy through the mitochondrial oxidative phosphorylation with low levels of free cytosolic NADPH (Moreira et al., 1995; Sallin et al., 2018). However, the levels of NADPH in cancer cells are 5–10 times higher compared with normal cells (Chiarugi et al., 2012). These high levels of NADPH may explain the anomalous characteristic of cancer cell metabolism first observed by Otto Heinrich Warburg (Vander Heiden et al., 2009; Warburg, 1956). The Warburg effect established increased glycolysis as a main source of metabolic fuel in tumor cells under hypoxic or even normoxic conditions. Particularly because perturbation of NADPH balance involved in a wide range of diseases such as diabetes and Alzheimer (Block, 2008; Gray et al., 2013), precisely monitoring is important for understanding and regulating the metabolic reprogramming in these diseases.

Currently, several conventional methods are widely used to quantify NADPH in cell extracts (Kupfer and Munsell, 1968; Lorenz et al., 2013; Lowry et al., 1961; Sies et al., 1977; Umemura and Kimura, 2005); these end-point assays are mostly based on microplate absorbance or

* Corresponding author. Department of Biological Sciences and Research Center of Ecomimetics, Chonnam National University, Gwangju, 61186, Republic of Korea.
E-mail address: eungsam.kim@chonnam.ac.kr (E.-S. Kim).

https://doi.org/10.1016/j.bios.2019.111753
Received 18 June 2019; Received in revised form 28 August 2019; Accepted 30 September 2019
Available online 1 October 2019

fluorescence spectrophotometry, mass spectrometry, and chromatography. However, these approaches are invasive and not able to detect the transient subcellular NADPH changes associated with metabolic activation or dysfunction in intact individual cells. Furthermore, all these methods suffer from potential NADPH oxidization or degradation during the sample processing. Alternatively, researchers have directly measured the weak autofluorescence of NAD(P)H to monitor the cellular redox state (Blacker and Duchen, 2016). Unfortunately, this method does not distinguish between NADH and its phosphorylated congener, NADPH, or between protein-bound and free nucleotides. To overcome these drawbacks, researchers have directly measured NAD(P)H with fluorescence lifetime imaging microscopy (FLIM) and genetically encoded NADPH fluorescence sensors in live mammalian or bacterial cells (Blacker et al., 2014; Goldbeck et al., 2018; Tao et al., 2017). FLIM requires mathematical modeling to quantify NADPH flux in living cells and is thus considered a complex way of detecting NAD(P)H in live cells (Blacker et al., 2014). Tao et al. used *in silico* computation of NADH nucleotide binding pocket that was subsequently mutated for NADPH specificity to measure the intracellular NADPH levels in living cells (Tao et al., 2017). Recently, the genetically encoded sensor has been introduced to estimate the concentration of NADPH which was released from bacterial cells whose cell membrane should be chemically permeabilized (Goldbeck et al., 2018). Although NADPH can be detected with genetically encoded fluorescence sensors in live cells, it required protein engineering or membrane-permeabilizing steps. Thus, a more straight forward NADPH assay is needed for tracking the relation between intracellular NADPH levels and cell metabolism or behaviors in nominal culture conditions without damaging cell integrity.

Previously, our group identified a metagenomic blue fluorescent protein (mBFP) from soil bacteria (Hwang et al., 2012; You et al., 2019). It was demonstrated that mBFP has no intrinsic fluorescence but shows significantly high blue fluorescence at 450 nm specifically on interaction with NADPH when excited at 350 nm. Because the fluorescence is attributed to the formation of mBFP-NADPH complex, we expected that mBFP could be a candidate biosensor for measuring NADPH in live cells. We confirmed that the fluorescence enhancement of the bacterial protein relies on its binding to NADPH only, not to other nicotine cofactors such as $NADP^+$, NADH, or NAD. In this work, we introduced the bacterial mBFP gene into human cancer cells to monitor NADPH dynamics not in the cell lysate but in live cells. Two-photon microscopy was employed to avoid photobleaching of mBFP-NADPH complexes or photodamage during the long-term live cell imaging. We could monitor the effects of the glucose concentration in the culture medium, treating with agents such as diamide and dehydroandrosterone (DHEA), and knockdown of G6PD transcripts on intracellular NADPH levels in mBFP-transfected cancer cells in real time.

2. Materials and methods

2.1. Materials

All reagent-grade chemicals including *N*, *N*-dimethylformamide (diamide), dehydroandrosterone (DHEA) were purchased from Sigma-Aldrich (St. Louis, MO, USA) unless otherwise mentioned. Transfection reagent Lipofectamine™ 3000, Dulbecco's Modified Eagle medium (DMEM) supplemented with 1000 mg/L glucose, and glucose-free DMEM were obtained from Invitrogen. Anti-mBFP antibody was kindly provided by Dr. Sung-Hwan You at Chonnam National University.

2.2. Plasmid construction

The mBFP gene was inserted into the *Eco*RV and *Eco*RI sites of pCS4+3FLAG DNA plasmid (Cat. No. 78769, Addgene) employed as a mammalian expression vector. PCR was performed with the cloning primer pair forward primer 5′-ATAGATATCATGCAGAATCTGAACGGCAAAGTGG-3′ and reverse primer 5′-ATAGAATTCTCAAGCGGCGAAGCCGC-3'.

2.3. Cell culture

HeLa cell (a human cervical cancer cell line from ATCC) was cultured as described previously (Mesnil et al., 1995). In brief, cells were grown in DMEM supplemented with 10% fetal bovine serum (FBS), 100 IU/ml penicillin, and 100 mg/ml streptomycin. All cells were cultured at 37 °C in a humidified atmosphere of 95% air and 5% CO_2.

2.4. Transfecting the mBFP gene into HeLa cells

For transient transfection, approximately 2.5×10^5 cells/ml were cultured on a 35-mm culture dish as described previously (Wang et al., 2018). The pCS4-mBFP plasmids were transfected with a transfection reagent, Lipofectamine™ 3000, according to the manufacturer's protocol with a DNA to Lipofectamine ratio of 1:3 w/v. A transfection enhancer, the 3000 enhancer reagent (1:2, DNA: Reagent, w/v), was used along with the Lipofectamine 3000 transfection reagent for all transfections. Typically, 2.5 μg of plasmid DNA were transferred to each 35-mm culture dish.

2.5. Knockdown of G6PD transcripts

To suppress G6PD expression, HeLa cells were transfected with small interfering RNA (siRNA) against human G6PD transcripts. The siRNA with its sequence of 5′-UGAUGCAGAACCACCUACU-3′ was synthesized and purified by Bioneer (Daejeon, Korea). The cells were transfected with G6PD siRNA at a final concentration of 50 nM in the presence of Lipofectamine™ 3000 reagent according to the manufacturer's instructions. After 72 h of transfection, the efficiency of G6PD knockdown was confirmed by Western blot analysis.

2.6. Western blotting

Cells were lysed in 1× SDS sample buffer supplemented with a protease/phosphatase inhibitor cocktail (Cell Signaling Technology, Danvers, MA, USA). Equal amounts of total protein (30–50 μg) were separated on SDS–PAGE and electrotransferred onto nitrocellulose membranes. Membranes were incubated with primary antibodies to mBFP, α-Tubulin (T6074, Sigma-Aldrich), and G6PD (#8866, Cell Signaling Technology) followed by secondary antibodies conjugated to horseradish peroxidase, then a chemiluminescence detection mixture (Roche) and imaging.

2.7. Immunocytochemistry

HeLa cells were grown on glass cover slips and transfected with pCS4-mBFP. At 48 h post-transfection, the cells were fixed for 10 min with 4% paraformaldehyde in 1× phosphate buffered saline (PBS), pH 7.4. The slides were washed 3 times for 5 min with 1× PBS and subsequently permeabilized in 0.3% Triton for 2 min followed by an additional washing. The slides were incubated with blocking solution (2% FBS in 1× PBS) for 1 h at room temperature, following a 1 h incubation with rabbit anti-mBFP diluted (1:200) in blocking solution. Goat anti-rabbit conjugated to Alexa Fluor 594 (A-21207, Invitrogen, Waltham, MA, USA) was diluted in blocking solution (1:500) and incubated for 1 h before the cover slips were mounted onto glass slides using ProLong Gold antifade reagent with DAPI (Life Technologies). Images were acquired using a laser confocal scanning microscope (TCS SP5 AOBS/TANDOM, Leica Microsystems, Germany).

2.8. Two-photon microscopy

We used two-photon fluorescence microscopy (TPM) with an intravital multi-photon microscope (SP8-MP, Leica) with a 25× 0.9 NA water

dipping objective lens. Cultured cells were kept at 37 °C using a temperature-controlled culture dish heater during image acquisition (Warner Instruments, Hamden, CT, USA). The mBFP-expressing cells were irradiated by InSight DS Plus laser system (Spectra-Physics, Santa Clara, USA) at the excitation wavelength of 750 nm. Time-lapse and 3D stack images of mBFP-mediated fluorescence were obtained by a spectral detector with a band filter with its wavelength range from 450 to 550 nm.

2.9. Treatment of cells with chemical inhibitors in glucose-conditioned medium

Before each treatment to cells grown on a 35-mm culture dish, the medium was removed, and cells were washed with pre-warmed 1× PBS. After fresh medium with no glucose was added, cells were incubated for 1 h at 37 °C. The chemical inhibitors diamide and DHEA were dissolved in distilled water and cell culture-tested DMSO, respectively. Chemical stocks were diluted in glucose-free (0 mM) or low-glucose (5 mM) culture medium just before their treatment to cells.

2.10. Quantifying fluorescence signals

We acquired all time-lapsed images at a frame rate of 1 frame/5 s, using the Leica viewer program to quantify the average fluorescence intensity from the region of interest (ROI) in the cytosol of fluorescent cells. After the treatment of chemicals to mBFP-transfected cells, the fluorescence intensity of ROIs was normalized to the fluorescence level obtained at the identical ROIs just before each treatment (i.e., at 0 min).

2.11. Quantifying NADPH in cell lysis via microplate assay

We measured NADPH in the 35-mm culture dishes using an NADP/NADPH assay kit (K347, BioVision, Milpitas, CA, USA) according to the manufacturer's instructions. Prior to the treatment of DHEA inhibitor, cells were washed with PBS and glucose-deprived for 1 h. After 30 min treatment of DHEA, cells lysates were extracted in 400 µL of the recommended extraction buffer, and 50 µL were processed following instructions for each duplicate. The absorbance at 450 nm was measured in on a microplate reader (Epoch, BioTek, Winooski, VT, USA).

2.12. Statistical analysis

Quantified fluorescence signals are presented as the mean ± S.D. for at least three independent experiments. We employed Student's t-test to analyze the statistical difference of two groups. $P < 0.05$ was considered statistically significant.

3. Results

3.1. Working principles to monitor intracellular NADPH levels using mBFP and TPM

It is known that the amount of glucose introduced into cells through glucose transporter (Glut) changes depending on the glucose concentration in the culture medium, resulting in a change in the production of NADPH by PPP (Gelman et al., 2018). For the proof of concept, we planned to perturb the NADPH in live cells through three biochemical treatments: diamide and DHEA as oxidizing reagents, low- or no-glucose media, and siRNA against G6PD; siRNA is a method that can be used to downregulate the amount of transcript of a specific gene in cells (Watts and Corey, 2012). As illustrated in Fig. 1, to visualize intracellular NADPH flux in live cells we utilized TPM, which allows better subcellular resolution and reduces photobleaching and photodamage during long-term imaging.

3.2. Enhancing NADPH fluorescence in mBFP-transfected cells

To validate the ability of bacterial mBFP in the detection of NADPH metabolism in mammalian cells, we transfected mBFP gene into HeLa cells. As an initial step, we characterized the expression of mBFP in HeLa

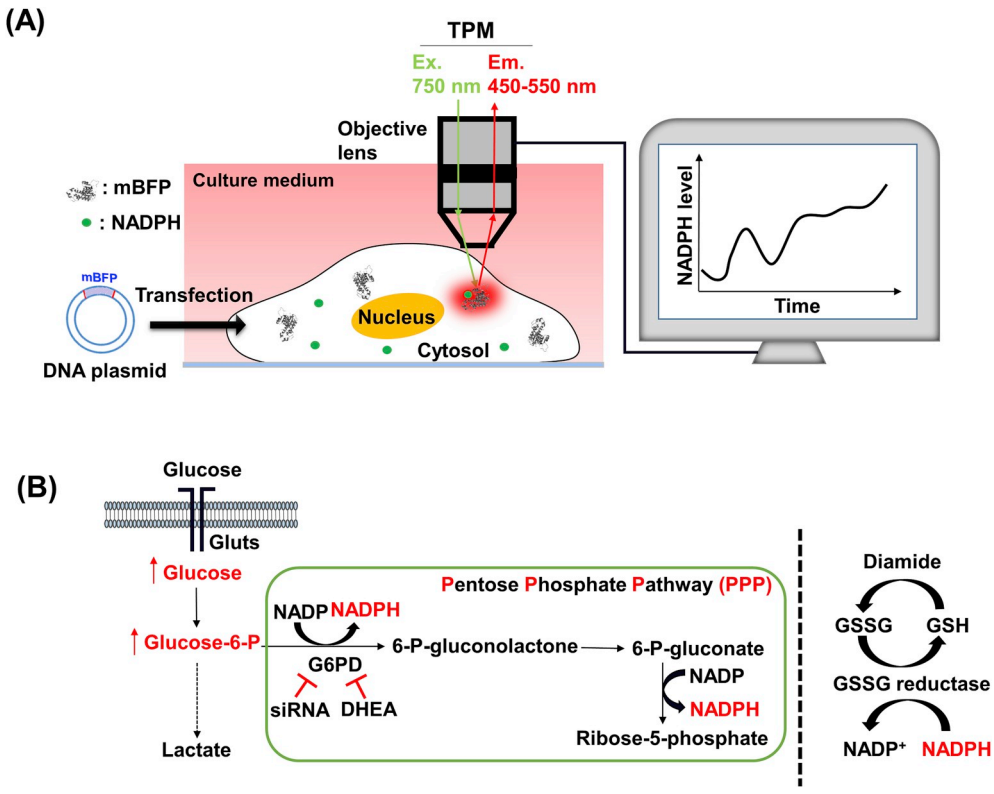

Fig. 1. Scheme for real-time monitoring of NADPH levels in live mammalian cells with NADPH-associated metabolic pathways. (A) The mBFP gene was expressed in the cytosol of HeLa cells after the transfection of the DNA plasmid. mBFP specifically binds to NADPH and enhances its intrinsic fluorescence. Time-lapsed two-photon microscopy was employed to excite NADPH at 750 nm and collect the enhanced fluorescence with its peak at 450 nm. The fluorescence signal was quantified to display the changes in intracellular NADPH levels in real time. **(B)** Through glucose transporters (Gluts), the glucose in the medium is transported into the cytosol, where it is metabolized to generate NADPHs for cellular redox homeostasis. DHEA, an inhibitor of mammalian G6PD, and G6PD-targeted siRNA were used to decrease the availability of NADPH in the PPP. Diamide treatment induced intracellular oxidation of glutathione (GSH), which rapidly converts NADPH to $NADP^+$ in cells.

cells by Western blot analysis and immunocytochemistry (Fig. S1). After 48 h post-transfection, Western blot revealed high mBFP expression in the cell protein, and immunocytochemistry with anti-mBFP antibody revealed the intracellular locations of the mBFP: The majority of mBFP expressed was cytoplasmic in distribution, as observed by confocal microscopy (Fig. S1B). Next, to visualize NADPH signals in living HeLa cells, we applied a wide range of excitation wavelengths from 680 to 790 nm in TPM (Fig. S2). The results obtained from the two-photon excitation showed maximum fluorescence intensity of mBFP-NADPH complex when the cells were excited at 750 nm, and consequently, we chose 750 nm for further detection of intracellular NADPH levels. These images demonstrate dark nuclear regions, as well as bright regions (red color), that correspond to NADPH in the cytoplasm, which has a higher fluorescence intensity (Fig. 2A). Importantly, although mBFP is bacterial in origin, we observed no significant changes in morphology or viability in the HeLa cells that expressed mBFP. In our tests, cytosolic NADPH signals increased about 10-fold in mBFP transfected cells in comparison with non-transfected cells (Fig. 2B). Taken together, these results confirm that mBFP is a functional protein that can be used for the real-time monitoring of intracellular NADPH flux in live mammalian cells.

3.3. Real-time monitoring of NADPH affected by diamide in low-glucose medium

To explore the effects of chemical inhibitors on intracellular NADPH flux, cells were deprived of glucose for 1 h and then treated with different concentrations of diamide in 5 mM glucose medium (Fig. 3A). We observed the intracellular NADPH flux for 20 min and normalized its fluorescence intensity to the first 2 min of samples without drug treatment in each experiment (Fig. 3B). Interestingly, when 5 mM glucose media was added to the cells, there was a 2-fold increase of NADPH intensity within 1 min (Fig. 3C); when these cells were treated with 10, 40, and 80 μM of diamide, a general oxidant, fluorescence signals decreased within 1 min and then gradually recovered in a dose-dependent manner. Treatment with diamide in the presence of glucose induced a 1.2-fold increase in NADPH levels within 20 min except in cells treated with 160 μM of diamide. This increase in NADPH may result from the presence of glucose sources that regenerate cytosolic NADPH levels. In the presence of glucose, the PPP metabolites supply glucose-6-phosphate to produce NADPH. However, the presence of glucose did not affect NADPH recovery when cells were treated with high doses of diamide. With 160 μM diamide, the fluorescence intensity immediately decreased and showed no recovery within 20 min; indeed, high doses of diamide strongly affected NADPH regeneration, and cells were not able to recover their NADPH levels.

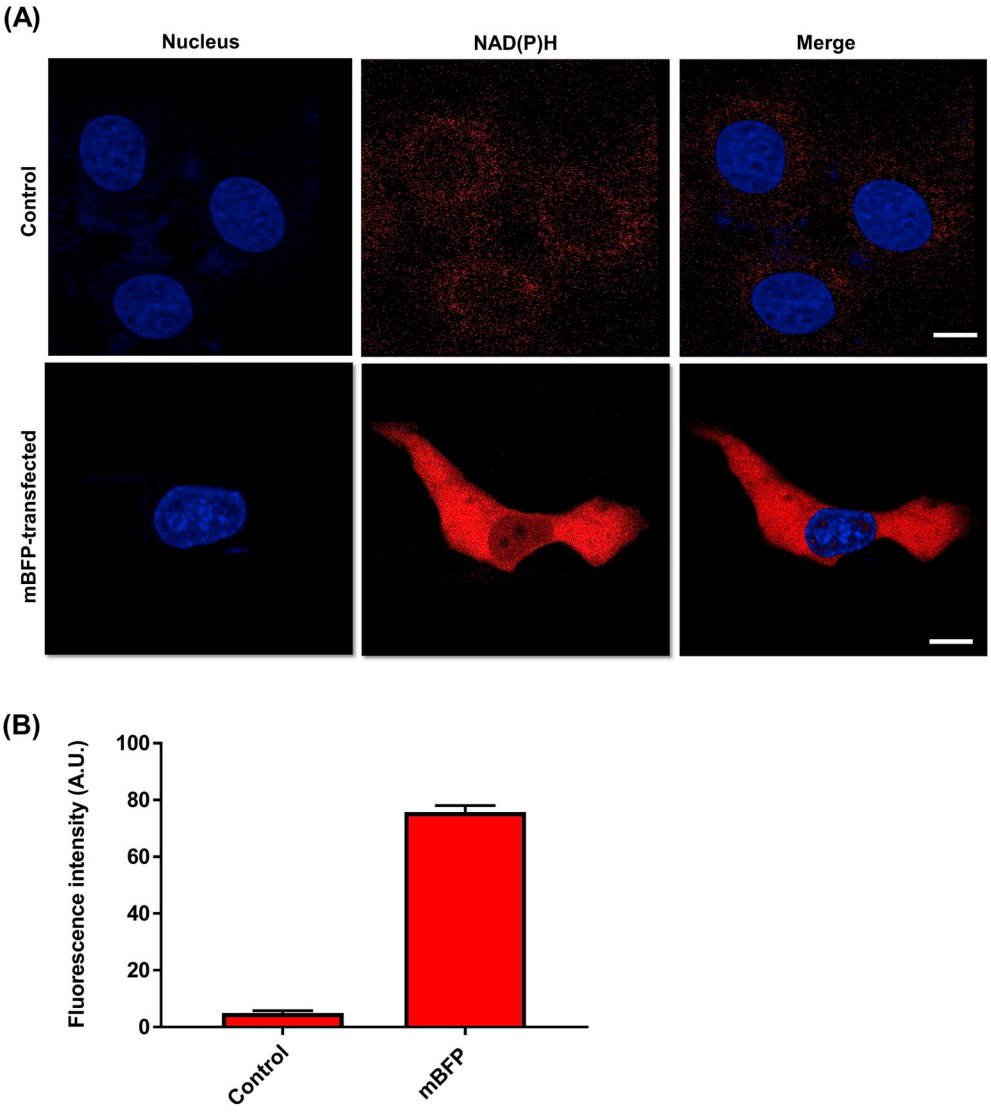

Fig. 2. Enhanced NADPH fluorescence in mBFP-transfected cells. (A) The fluorescence images of the nucleus (blue) and NAD(P)H (red) in control and mBFP-transfected HeLa cells are merged in the third column. **(B)** Comparison of NADPH fluorescence intensity between control and mBFP-transfected cells. Scale bars: 80 μm. Error bars indicate mean ± S.D. (n = 10). (For interpretation of the references to color in this figure legend, the reader is referred to the Web version of this article.)

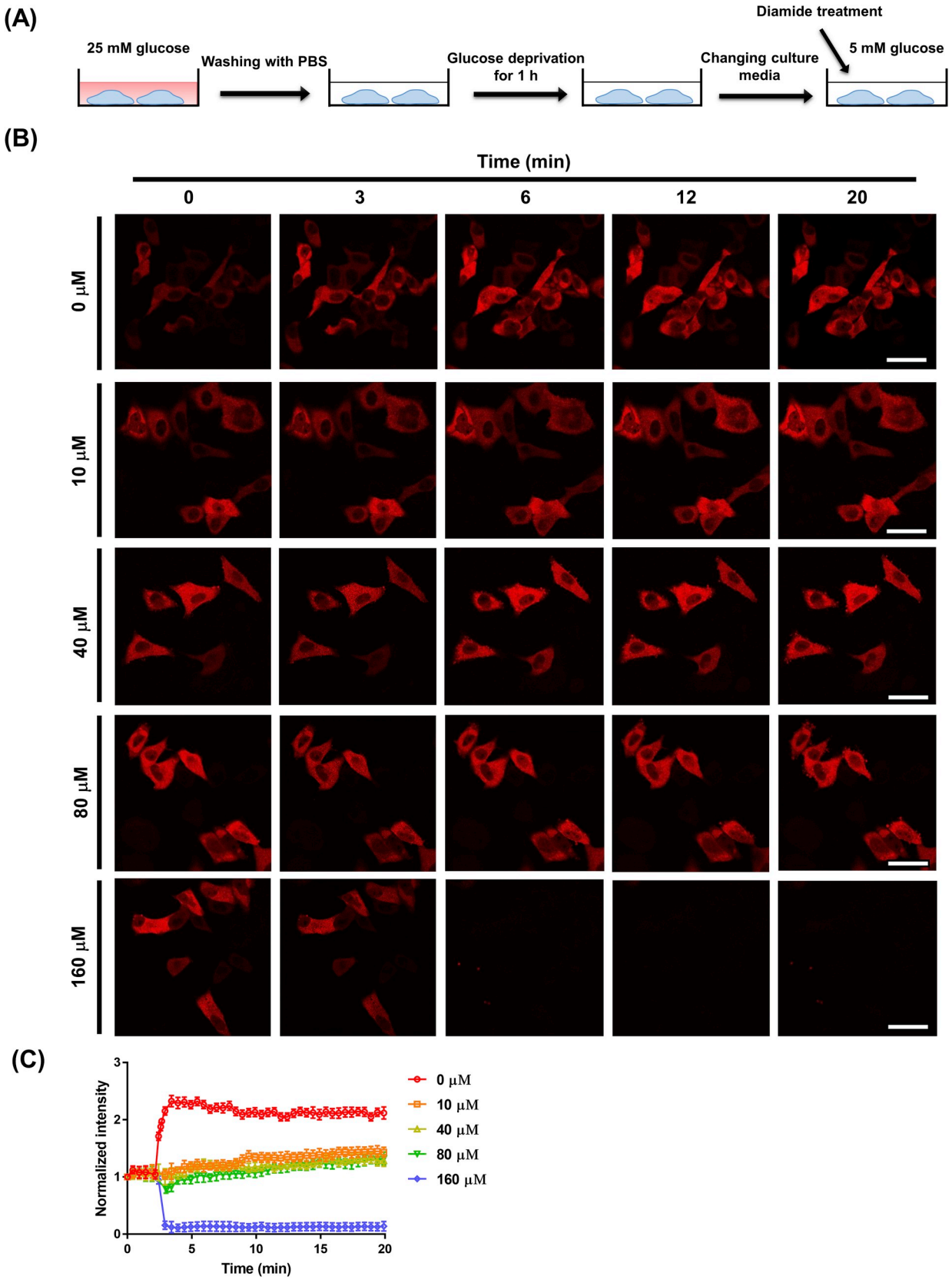

Fig. 3. Visualization of intracellular NADPH flux in response to diamide in low-glucose culture medium. (A) Prior to the diamide treatment, cells were washed with PBS and deprived of glucose for 1 h. **(B)** Changes in NADPH fluorescence intensity in HeLa cells with different concentrations of diamide in the culture medium with 5 mM glucose (time-lapse video files for each 20-min imaging session are available in Supplementary Materials). Scale bars: 80 μm. **(C)** Normalized kinetic profiles of NADPH flux in response to diamide treatment. All data were normalized to the first 2 min fluorescence level of samples without chemical treatment in each experiment.

3.4. Real-time monitoring of NADPH affected by diamide in glucose-free medium

To investigate more about the correlation between glucose sources and NADPH levels under treatment of diamide, cells were deprived of glucose for 1 h and then treated with different concentrations of diamide dissolved in glucose-free medium. First, to consider the effect of glucose on NADPH levels, we obtained the fluorescence signals for 20 min in cells with glucose-free medium (Fig. 4A) but observed no significant changes in NADPH levels (Fig. 4B). In glucose-deprived cells, adding 10 and 40 μM of diamide dose-dependently and rapidly decreased the fluorescence intensity of NADPH within 2–3 min (Fig. 4A and B); in contrast, NADPH fluorescence recovered more slowly than it did in cells treated with 5 mM glucose. Notably, when these cells were treated with 80 μM of diamide, the NADPH signals decreased in less than 1 min and only some of the cells were able to recover their NADPH levels within 20 min. Moreover, the addition of 160 μM diamide, rapidly decreased the fluorescence signal in less than 30 s. Indeed, with 160 μM diamide, in both the presence and absence of glucose, cells were not able to recover their NADPH levels within 20 min.

3.5. Real-time monitoring of NADPH affected by DHEA, a G6PD inhibitor

To better understand the role of the PPP in generating cytosolic NADPH, we investigated the function of G6PD in HeLa cells; G6PD is a key protective enzyme responsible for maintaining adequate levels of the major cellular reducing agent NADPH, which is needed for reducing folic acid to tetrahydro folic acid as well as for ribonucleotide and thymidylate synthesis. Therefore, as the PPP inhibited G6PD function, the cells were deprived of glucose for 1 h and then treated with trans-DHEA in the presence or absence of 5 mM glucose (Fig. 5A): With 200 μM DHEA, there was an approximately 50% decline in NADPH signal within 3 min (Fig. 5B and C). Our result showed that when the cells had sufficient glucose sources in media, they recovered about 5% of their NADPH levels within 15 min. However, in the absence of glucose, DHEA strongly inhibited NADPH production, and cells were not able to recover their NADPH levels within 20 min. These data demonstrate that NADPH flux is markedly affected by glucose metabolism when G6PD is inhibited by DHEA in HeLa cells.

3.6. Real-time monitoring of NADPH in G6PD-knockdown cells

Alternatively, we investigated metabolic alterations caused by siRNA-mediated G6PD knockdown. After 72 h of siRNA transfection, the efficiency of G6PD knockdown was confirmed by Western blot analysis (Fig. S3). G6PD converts G6P and $NADP^+$ to 6 PG and NADPH. In accordance, treatment with 40 μM diamide resulted in a 50%–60% reduction of NADPH levels in G6PD knockdown cells containing 5 and 0 mM glucose sources (Fig. 6A and B). Of note, in the presence of 5 mM glucose, NADPH level was recovered about 2%–3% in G6PD knockdown cells after 20 min but not in cells cultured in glucose-free medium (Fig. 6C). These results suggest that G6PD is essential for cellular NADPH production in HeLa cells.

4. Discussions

Real-time monitoring of intracellular NADPH levels in live cells has been limited by few available biosensors (Goldbeck et al., 2018; Tao et al., 2017; Tu et al., 2014). Here, for the first time, we demonstrated that bacterial metagenome-derived blue fluorescent protein (mBFP) can be used effectively for this monitoring in live mammalian cells in which the mBFP gene could be expressed and bind to NADPH, which resulted in an approximately 10-fold enhancement of NADPH fluorescence compared with non-transfected mBFP cells. We also monitored the effects of the glucose concentration of with culture medium and treatment with oxidizing agents such as diamide, which rapidly decreased the fluorescence signal of NADPH (less than 30 s). We further showed that DHEA and knockdown of G6PD transcripts induced a 50% decline in NADPH levels with no significant recovery within 15 min in live cancer cells. These results suggest that bacterial mBFP is a functional protein that can be expanded to a platform to track the spatio-temporal changes in NADPH levels in live cells in real time.

Fluorescence lifetime imaging microscopy (FLIM) and several genetically encoded fluorescent sensors have been developed to study the dynamics of NAD(P)H levels. FLIM entails multi-parameter analysis to quantify and detect NADPH flux in living cells, which requires precise measurement of cell fluorescence decay profiles (Blacker et al., 2014). They showed that glucose deprivation in HEK293 cells reduced intracellular NAD(P)H by 10%–15% in live cells using FLIM. In this study, we also confirmed that when HeLa cells were deprived of glucose for 1 h, intracellular NADPH decreased by 10%–15% within 10 min under mBFP-mediated fluorescence (Fig. S4). Recently, *in silico* computation of a NADH nucleotide binding protein and subsequent high-throughput screening generated candidates for the genetically engineered NADPH biosensor (Tao et al., 2017). Our mBFP originated from soil bacteria was able to directly and specifically bind to NADPH in the cytoplasm without any genetic mutation. A *Vibrio*-originated NADPH reporter protein (called mBFP *Vibrio vulnificus*) was applied to plant tissues (Tu et al., 2014), not showing significant change in NADPH levels in subcellular compartments where the reporter was targeted. This mBFP has been used to measure the concentrations of NADPH released from bacterial cells after the treatment of cetyl trimethylammonium bromide (CTAB), a membrane-permeabilizing agent (Goldbeck et al., 2018). However, our approach could monitor intracellular NADPH levels without damaging the structural integrity of cell membranes. These results strongly support our mBFP can act as an NADPH sensor in live cells under metabolically perturbed conditions.

To understand more thoroughly the correlation between glucose and NADPH production in cancer cells, cells were starved of glucose for 1 h and then treated with different chemical inhibitors in 5 mM of glucose. Of note, we could observe the shrinkage of cell boundary when the cell was incubated in glucose-free medium for 2 h and more (Fig. S5). Therefore, to prevent cell apoptosis in HeLa cells, we limited the duration of glucose starvation to 1 h and monitored the intracellular NADPH level for 30 min at maximum. Diamide is an effective reagent for the intracellular oxidation of glutathione that leads to rapid conversion of NADPH to $NADP^+$ in less than 1 min (Kosower et al., 1969). In glucose-deprived HeLa cells that were treated with different concentrations of diamide, NADPH decreased and then gradually recovered within 1–2 min in the presence of 5 mM glucose. This recovery of NADPH can be explained by the enhancement of NADPH regeneration as a consequence of G6PD activation in the PPP when glucose was available in media. It is known that cancer cells take up and metabolize glucose to a greater extent than normal cells and may upregulate glucose metabolism to produce more pyruvates and NADPHs to protect against hydrogen peroxide-induced toxicity (Riganti et al., 2012). Because NADPH can be generated through several mechanisms, recent flux analysis indicated that cytosolic NADPH is mainly provided by oxidative PPP (Riganti et al., 2012). However, NADPH biosynthesis in different glucose conditions with the shutdown of glucose uptake is still unclear. To further study this correlation, in this work, we investigated inhibiting G6PD with both the chemical inhibitor DHEA and siRNA targeted to G6PD for metabolic alteration. DHEA is an adrenal steroid hormone and well-known uncompetitive inhibitor of mammalian G6PD that reduces the availability of NADPH (Riganti et al., 2012), and DHEA inhibition of G6PD led to a 50% reduction in NADPH levels (Fig. 6B and C). Furthermore, we showed that the presence of 5 mM glucose could slightly recover NADPH levels in HeLa cells. Although this slight increase was merely 2%–5%, it remained in the cells in which siRNA inhibited G6PD inhibited through siRNA and that were then treated with 40 μM diamide. These data strongly indicate that the presence of glucose elevates the production of NADPH in metabolically perturbed cancer

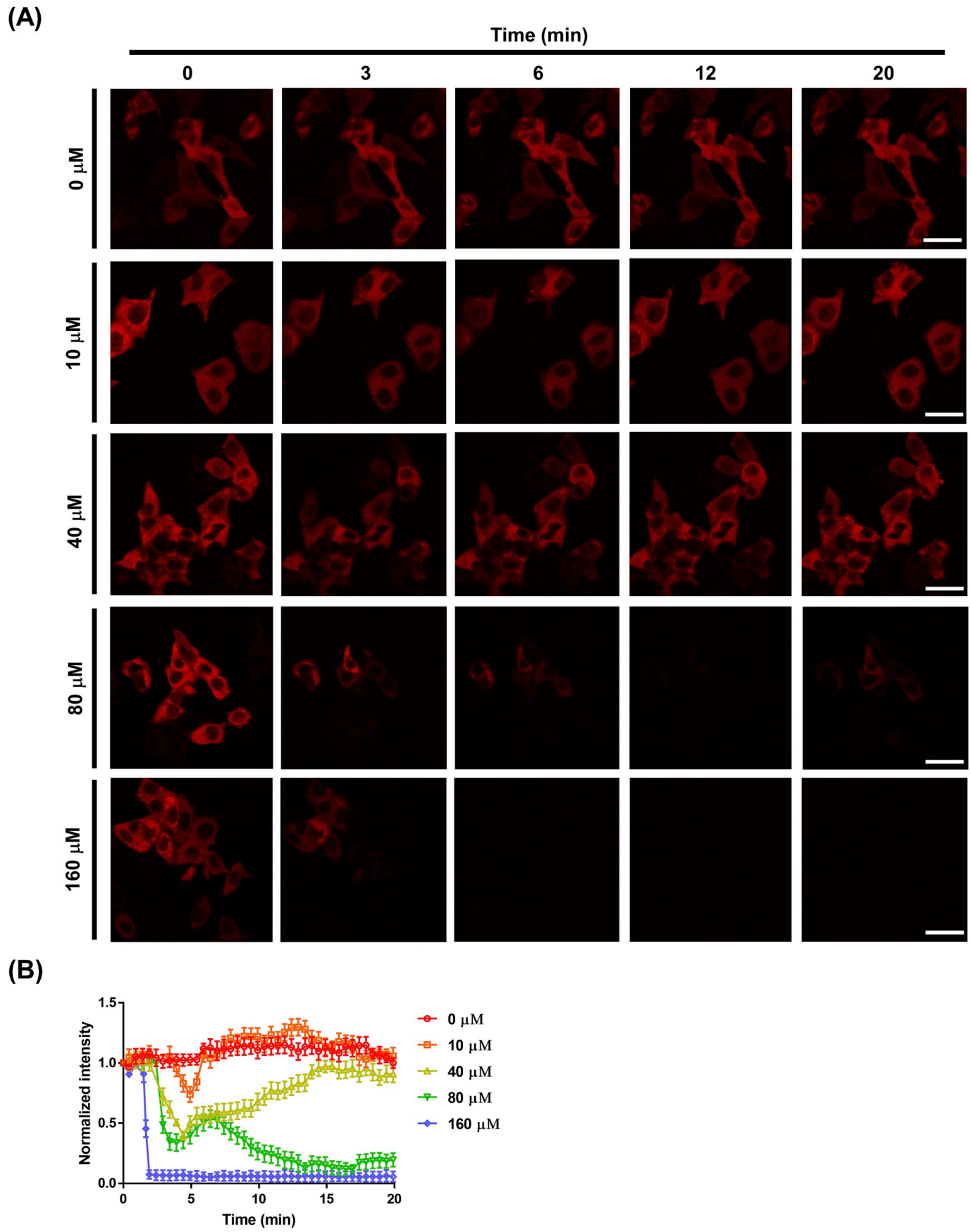

Fig. 4. Monitoring the effect of diamide on NADPH regeneration in glucose-deprived cells. (A) Changes in NADPH fluorescence intensity in HeLa cells at different concentrations of diamide in the glucose-free medium. Scale bars: 80 μm. **(B)** Normalized kinetic profiles of NADPH flux in response to diamide treatment. All data were normalized to the first 2 min fluorescence level of samples without chemical treatment in each experiment.

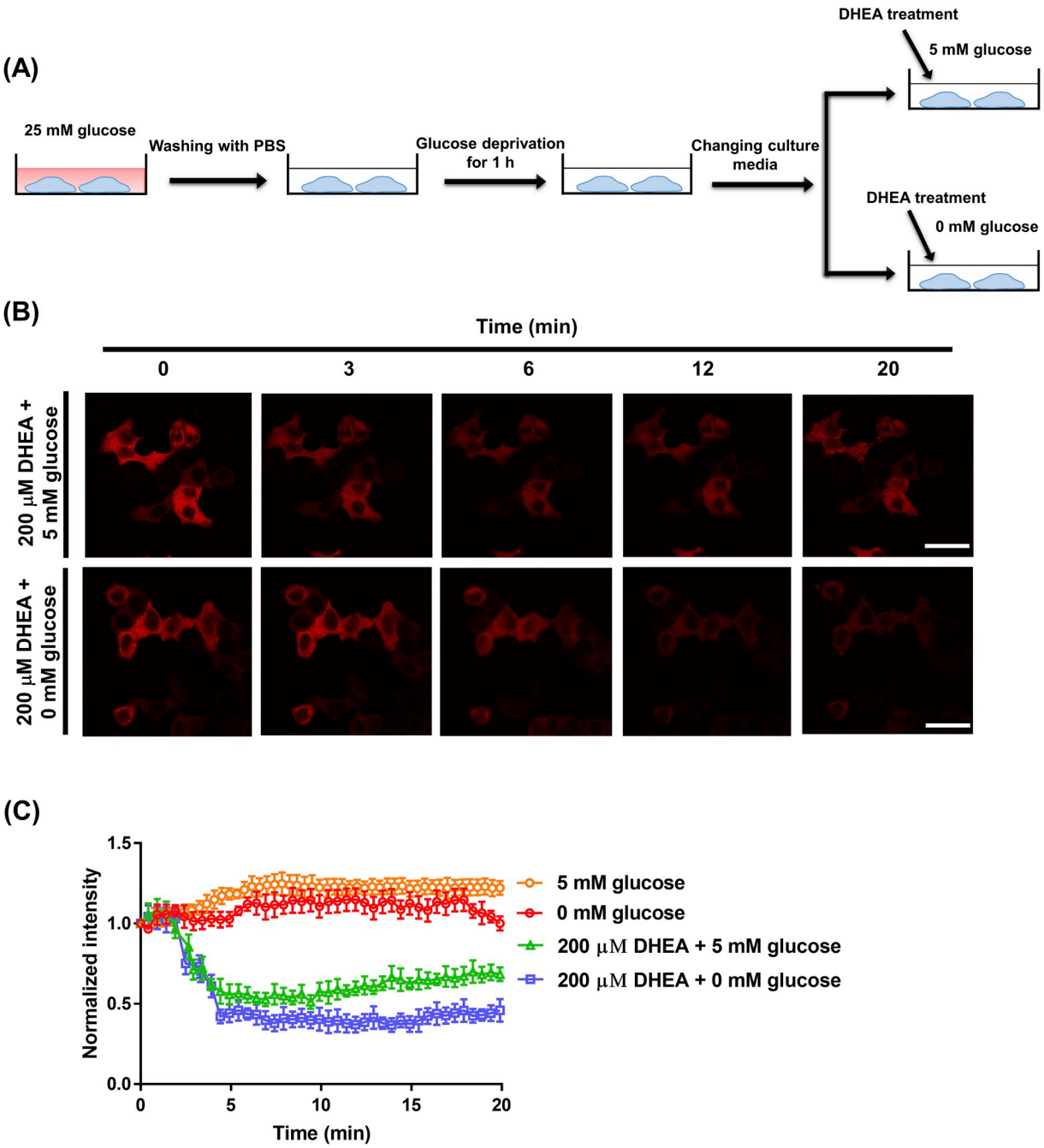

Fig. 5. Monitoring the effects of the chemical inhibition of DHEA on intracellular NADPH levels. (A) Prior to the treatment with 200 μM DHEA and glucose-conditioned medium, cells were washed with PBS and deprived of glucose for 1 h. **(B)** Changes in NADPH fluorescence intensity in HeLa cells with 200 μM DHEA in glucose-free (lower row) or low-glucose (upper row) medium. Scale bars: 80 μm. **(C)** Normalized kinetic profiles of NADPH flux in response to 200 μM of DHEA in the glucose-conditioned medium. All data were normalized to the first 2 min fluorescence level of samples without chemical treatment in each experiment.

cells.

Based on our observations of the effects of glucose in NADPH production, we aimed to monitor the NADPH levels in HeLa cells treated with diamide and/or DHEA in the absence of glucose sources in culture media. When these cells were treated with the different diamide concentrations in the absence of glucose, NADPH fluorescence recovered more slowly than it did in cells treated in 5 mM glucose medium. Additionally, there was no NADPH recovery when cells were treated with 160 μM of diamide whether glucose existed or not. Based on these results, glucose sources played an important role in the recovery of NADPH production when cells were treated with low levels of diamide, but under high oxidative stress, diamide inhibited the recovery of intracellular NADPH levels.

Furthermore, we applied a commercially available *in-vitro* assay kit to measure the NADPH concentration of HeLa cells under the same condition as for live-cell NADPH imaging (Fig. S6): The total NADP ($NADP^+$ and NADPH) is extracted in the cells, and then most of the $NADP^+$ is destroyed by heating the extracts at 60 °C following a previous report (Wu et al., 1986). We showed that adding 5 mM glucose to HeLa cells induced 50%–60% production of NADPHs within 30 min. However, when these cells were treated with DHEA inhibitor, it reduced NADPH by 50% and 20%, respectively, with and without glucose in the culture medium. Of note, we were able to detect NADPH signals for every single cell in the live cell monitoring of NADPH levels, but *in-vitro*

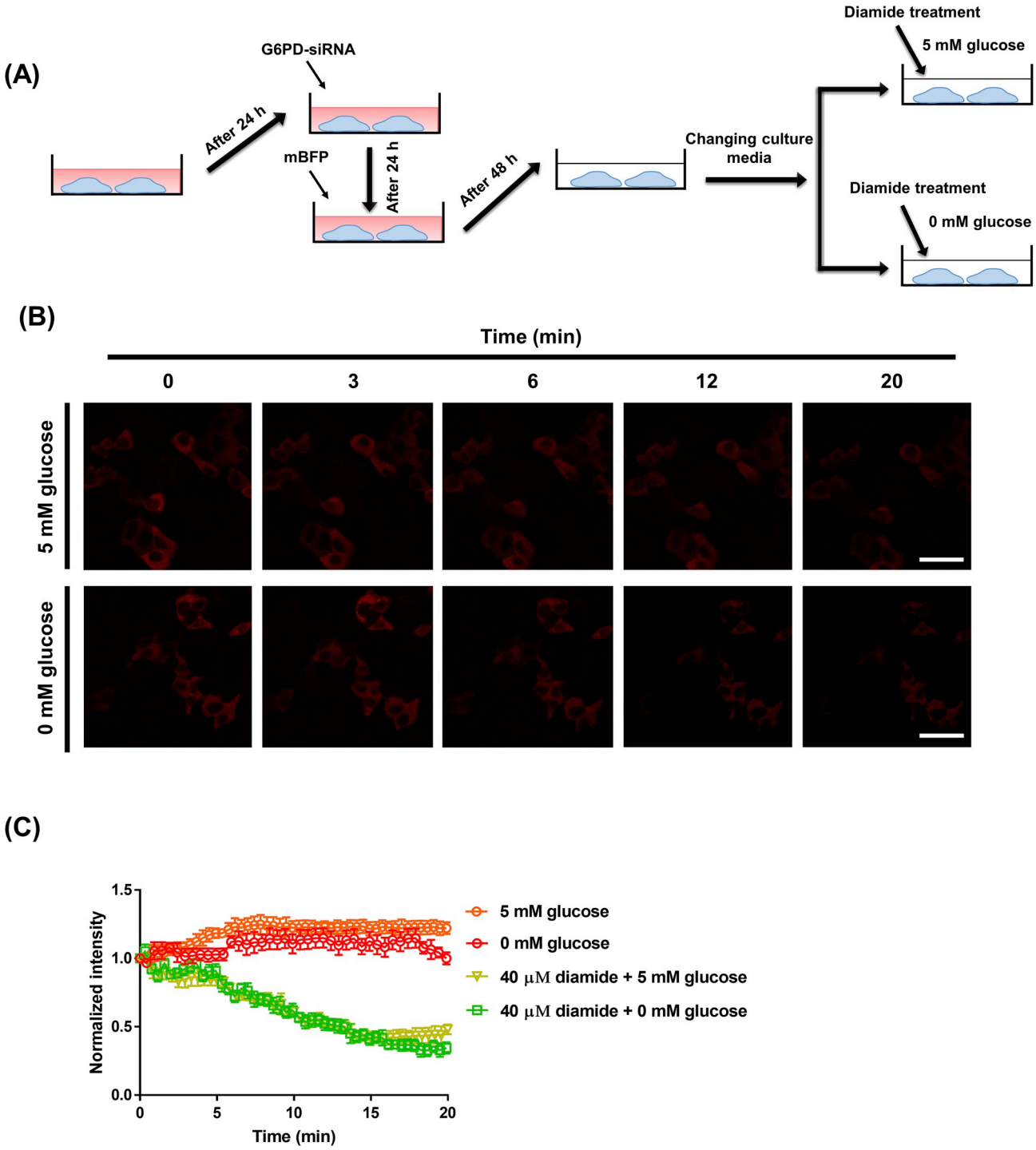

Fig. 6. Monitoring the decay of the NADPH level in G6PD knockdown cells on treatment with a chemical inhibitor. (A) Transfection scheme for G6PD siRNA and mBFP gene in HeLa cells. After 48 h post-transfection, cells were treated with 40 μM diamide in glucose-conditioned medium. **(B)** Changes in NADPH fluorescence intensity in G6PD knockdown cells with 40 μM diamide in low-glucose (upper row) or glucose-free medium (lower row). Scale bars: 80 μm. **(C)** Normalized kinetic profiles of NADPH flux. All data were normalized to the first 2 min fluorescence level of samples without chemical treatment in each experiment.

NADPH measurement was limited to detecting total cell numbers; therefore, we were not able to observe dynamic changes in NADPH levels in HeLa cells after treatment with the oxidizing agents. Because the heating process and preparation steps can have negative effects on intracellular NADPH, it is difficult to reliably measure and detect NADPH concentrations in lysed cells. Taken together, real-time imaging using mBFP in HeLa cells not only allows for fast and convincing detection of NADPH in individual cells but also shows large dynamic changes, warranting further research with multiple implications for monitoring NADPH levels in cancer cells.

We applied our proposed assay in three representative mammalian cell lines: human embryonic kidney (HEK293T), *Cercopithecus aethiops* kidney (COS-7), and Caucasian fetal lung fibroblast cells (WI-26) (Figs. S7, S8 and S9). Being consistent with the NADPH profiles obtained in HeLa cells, it is concluded that mBFP is a functional protein that can be used for the real-time monitoring of intracellular NADPH flux in other living mammalian cells. It should be noted that mBFP also has its own limitations. First, we used viral particles to stably express the mBFP gene

in two different cell lines, but despite several attempts, we failed to generate stable cell lines that overexpressed our gene in HeLa and A549 cells. Second, the non-targeted mBFP will not permit measuring NADPH concentrations in organelles such as mitochondria or chloroplast. Genetic engineering of mBFP will enable us to target the NADPH biosensor to specific organelles in live animal or plant cells.

5. Conclusion

Introducing mBFP to mammalian cells allowed for long-term monitoring of intracellular NADPH in real time with low photobleaching, large dynamic ranges, and fast detection, which will enable us to monitor spatial-temporal changes in NADPH levels in single cells. Furthermore, we expect that it will be possible to understand the critical role of NADPH in both normal and pathological conditions in animal and plant tissues throughout the straightforward real-time monitoring of dynamic changes of intracellular NADPH using mBFP as a genetically encoded biosensor.

Declaration of competing interest

The authors declare that they have no known competing financial interests or personal relationships that could have appeared to influence the work reported in this paper.

CRediT authorship contribution statement

Amir Roshanzadeh: Conceptualization, Investigation, Writing - original draft, Formal analysis. **Hyuno Kang:** Methodology, Formal analysis. **Sung-Hwan You:** Conceptualization, Resources. **Jaehong Park:** Investigation, Validation. **Nguyen Dang Khoa:** Writing - review & editing, Visualization. **Dong-Hyun Lee:** Conceptualization, Writing - review & editing. **Geun-Joong Kim:** Conceptualization, Writing - review & editing. **Eung-Sam Kim:** Conceptualization, Supervision, Writing - review & editing, Project administration.

Acknowledgments

This work was supported by National Research Foundation of Korea grants funded by the Korean Ministry of Science and ICT and the Ministry of Education (grant nos. NRF-2018R1A4A1023882, NRF-2018R1D1A3B07049282, and NRF-2015R1C1A1A01052498). The authors acknowledged the financial support through the Intelligent Synthetic Biology Center (NRF-2017030616) program of the National Research Foundation (NRF) funded by the Ministry of Science, ICT and Future Planning and also supported by a grant from the Marine Biotechnology Program (20170305), funded by the Ministry of Oceans and Fisheries, Korea. Two-photon microscopy was performed at the Gwangju Center at the Korea Basic Science Institute.

Appendix A. Supplementary data

Supplementary data to this article can be found online at https://doi.org/10.1016/j.bios.2019.111753.

References

Blacker, T.S., Duchen, M.R., 2016. Investigating mitochondrial redox state using NADH and NADPH autofluorescence. Free Radic. Biol. Med. 100, 53–65.
Blacker, T.S., Mann, Z.F., Gale, J.E., Ziegler, M., Bain, A.J., Szabadkai, G., Duchen, M.R., 2014. Separating NADH and NADPH fluorescence in live cells and tissues using FLIM. Nat. Commun. 5, 3936.
Block, M.L., 2008. NADPH oxidase as a therapeutic target in Alzheimer's disease. BMC Neurosci. 9 (Suppl. 2). S8-S8.
Chiarugi, A., Dolle, C., Felici, R., Ziegler, M., 2012. The NAD metabolome–a key determinant of cancer cell biology. Nat. Rev. Cancer 12 (11), 741–752.
Dröge, W., 2002. Free Radicals in the physiological control of cell function. Physiol. Rev 82 (1), 47–95.
Gelman, S.J., Naser, F., Mahieu, N.G., McKenzie, L.D., Dunn, G.P., Chheda, M.G., Patti, G.J., 2018. Consumption of NADPH for 2-HG synthesis increases pentose phosphate pathway flux and sensitizes cells to oxidative stress. Cell Rep. 22 (2), 512–522.
Goldbeck, O., Eck, A.W., Seibold, G.M., 2018. Real time monitoring of NADPH concentrations in corynebacterium glutamicum and Escherichia coli via the genetically encoded sensor mBFP. Front. Microbiol. 9 (2564).
Gray, S.P., Di Marco, E., Okabe, J., Szyndralewiez, C., Heitz, F., Montezano, A.C., de Haan, J.B., Koulis, C., El-Osta, A., Andrews, K.L., Chin-Dusting, J.P., Touyz, R.M., Wingler, K., Cooper, M.E., Schmidt, H.H., Jandeleit-Dahm, K.A., 2013. NADPH oxidase 1 plays a key role in diabetes mellitus-accelerated atherosclerosis. Circulation 127 (18), 1888–1902.
Hwang, C.-S., Choi, E.-S., Han, S.-S., Kim, G.-J., 2012. Screening of a highly soluble and oxygen-independent blue fluorescent protein from metagenome. Biochem. Biophys. Res. Commun. 419 (4), 676–681.
Kosower, N.S., Kosower, E.M., Wertheim, B., Correa, W.S., 1969. Diamide, a new reagent for the intracellular oxidation of glutathione to the disulfide. Biochem. Biophys. Res. Commun. 37 (4), 593–596.
Kupfer, D., Munsell, T., 1968. A colorimetric method for the quantitative determination of reduced pyridine nucleotides (NADPH and NADH). Anal. Biochem. 25, 10–16.
Lorenz, M.A., El Azzouny, M.A., Kennedy, R.T., Burant, C.F., 2013. Metabolome response to glucose in the ne nucleotides (NADPH and NADH). Anal. Biochem. 25 (15), 10923–10935, 1288.
Lowry, O.H., Passonneau, J.V., Schulz, D.W., Rock, M.K., 1961. The measurement of pyridine nucleotides by enzymatic cycling. J. Biol. Chem. 236, 2746–2755.
Mesnil, M., Krutovskikh, V., Piccoli, C., Elfgang, C., Traub, O., Willecke, K., Yamasaki, H., 1995. Negative growth control of HeLa cells by connexin genes: connexin species specificity. Cancer Res. 55 (3), 629–639.
Moreira, J.d.V., Hamraz, M., Abolhassani, M., Bigan, E., Pub, O., Willecke, K., Yamasaki, H., eit-Dahm, K.A., 1995. Negative growth control of HeLa cells by connexin genes: connexin species specificity. Cancer Res. 55 (3), 629–639.
Patra, K.C., Hay, N., 2014. The pentose phosphate pathway and cancer. Trends Biochem. Sci. 39 (8), 347–354.
Riganti, C., Gazzano, E., Polimeni, M., Aldieri, E., Ghigo, D., 2012. The pentose phosphate pathway: an antioxidant defense and a crossroad in tumor cell fate. Free Radic. Biol. Med. 53 (3), 421–436.
Sallin, O., Reymond, L., Gondrand, C., Raith, F., Koch, B., Johnsson, K., 2018. Semisynthetic biosensors for mapping cellular concentrations of nicotinamide adenine dinucleotides. Elife 7.
Schulze, A., Harris, A.L., 2012. How cancer metabolism is tuned for proliferation and vulnerable to disruption. Nature 491 (7424), 364–373.
Sies, H., Akerboom, T.P.M., Tager, J.M., 1977. Mitochondrial and cytosolic NADPH systems and isocitrate dehydrogenase indicator metabolites during ureogenesis from ammonia in isolated rat hepatocytes. Eur. J. Biochem. 72 (2), 301–307.
Smolke, C., 2009. The Metabolic Pathway Engineering Handbook: Tools and Applications. CRC Press.
Tao, R., Zhao, Y., Chu, H., Wang, A., Zhu, J., Chen, X., Zou, Y., Shi, M., Liu, R., Su, N., Du, J., Zhou, H.M., Zhu, L., Qian, X., Liu, H., Loscalzo, J., Yang, Y., 2017. Genetically encoded fluorescent sensors reveal dynamic regulation of NADPH metabolism. Nat. Methods 14 (7), 720–728.
Tu, J.-M., Chang, M.-C., Huang, L.L.H., Chang, C.-D., Huang, H.-J., Lee, R.-H., Chang, C.-C., 2014. The blue fluorescent protein from Vibrio vulnificus CKM-1 is a useful reporter for plant research. Bot. Stud. 55 (1), 79.
Umemura, K., Kimura, H., 2005. Determination of oxidized and reduced nicotinamide adenine dinucleotide in cell monolayers using a single extraction procedure and a spectrophotometric assay. Anal. Biochem. 338 (1), 131–135.
Vander Heiden, M.G., Cantley, L.C., Thompson, C.B., 2009. Understanding the Warburg effect: the metabolic requirements of cell proliferation. Science 324 (5930), 1029–1033.
Wang, T., Larcher, L.M., Ma, L., Veedu, R.N., 2018. Systematic screening of commonly used commercial transfection reagents towards efficient transfection of single-stranded oligonucleotides. Molecules 23 (10).
Warburg, O., 1956. On respiratory impairment in cancer cells. Science 124 (3215), 269–270.
Watts, J.K., Corey, D.R., 2012. Silencing disease genes in the laboratory and the clinic. J. Pathol. 226 (2), 365–379.
Wu, J.T., Wu, L.H., Knight, J.A., 1986. Stability of NADPH: effect of various factors on the kinetics of degradation. Clin. Chem. 32 (2), 314–319.
You, S.-H., Lim, H.-D., Cheong, D.-E., Kim, E.-S., Kim, G.-J., 2019. Rapid and sensitive detection of NADPH via mBFP-mediated enhancement of its fluorescence. PLoS One 14 (2), e0212061.